Mirko Dinulović

Full Professor
University of Belgrade
Faculty of Mechanical Engineering

Boško Rašuo

Full Professor
University of Belgrade
Faculty of Mechanical Engineering

Nikola Slavković

Professor
Academy of Applied Technical Studies
Belgrade

Đorđe Karić

Professor
Academy of Applied Technical Studies
Belgrade

Analysis of Aspect and Taper Ratio on Aeroelastic Stability of Composite Shells

In the present paper, the dynamic and static stability of composite shells for different aerodynamic configurations is investigated. Based on the existing models for flutter and torsional divergence, modified to include material anisotropy, stability parameters have been calculated for different aspects and taper ratios of the lifting (control) surface configurations. It was found that the methodology presented is a very effective method for stability analysis in preliminary design phases when a large number of cases have to be analyzed from the aspect of aerodynamics and flight conditions.

Keywords: *static stability, divergence, flutter, dynamic stability, computational flutter analysis, composites.*

1. INTRODUCTION

In the present paper, the effect of aspect and taper ratio on the overall stability of composite plates is inves–tigated. During the flight, within the flight envelope, as a result of inertial, aerodynamic, and elastic forces' constant interaction, a loss of stability might occur. This may potentially lead to stability loss which further leads to loss of control and, in certain cases, to disastrous airframe components failure with a catastrophic outcome (flight vehicle destruction).

It is of paramount importance that the stability ana–lysis of plates and shells is analyzed even in the early stages of the design since these components represent the main building block of any flight-worthy vehicle, manned and unmanned. This might particularly interest components such as missile fins and stabilizing surfaces.

The effect of aspect and taper ratio on the overall stability loss of thin plates used as stabilizing and con–trol surfaces is investigated. For different geometries by varying geometry parameters within the practical limits of the design, different geometries are analyzed. Parameters used to evaluate the aspect, and taper effects are expressed in terms of flutter velocities(V_f), stability margin (cal), drag coefficient increase (C_x), and divergence velocity (Vdiv). Modern aircraft structures are very flexible, and airframe flexibility makes aero–elastic studies, both dynamic and static, make an im–portant aspect of aircraft design and verification pro–cedures.

Arising from the interaction of elastic, inertial, and aerodynamic forces, acting on anelastic body, flutter is considered to be a dynamic aeroelastic instability that is characterized by the sustained oscillation of structure. The capability of a structure to sustain these oscillations is usually expressed using flutter speed as a measure of structural stability and represents the maximal speed at which the structure is considered to be stable. Above the

flutter speed, the structure becomes unstable and may lead to structural failure. Many current standards require that the flutter velocity is at least 20% higher than the flight "never exceed speed" (VNE).

Apart from flutter, another aeroelastic phenomenon (static) that designers should take into account is divergence. As for flutter, the divergence has an asso–ciated speed at which this phenomenon might occur. Potentially, divergence might lead to a structural failure as well. Divergence speed (Vdiv), like flutter speed, must reside well above the flight envelope for all flight-worthy vehicles. Throughout history, early airplanes had major divergence problems, like the Langley airplane and the Wright brothers' plane. Requirements for diver–gence speeds are also regulated through modern stan–dards currently in use. Hence, in structure analysis, it is of great importance to predict the divergence speed since it provides a useful measure of the general (torsi–onal) stiffness level of the plate and shell structure. In general, modern airplanes, due to proper design and stiffer materials, have divergence speeds higher than flutter speeds.

Structural stiffness is relatively low for flexible plates and shells. These structures are, therefore, more susceptible to instabilities even at low flow velocities. In this case, divergence and flutter can easily occur at relatively low velocities.

Because of their intrinsic property to be tailored to a specific function, composite materials are extensively used in the aerospace industry. Compared to metals, they have low specific weight, high specific modulus, and extremely high values of strength. It has become customary, in recent years, that many airframe compo–nents are designed and produced from composite mate–rials. One type of composite material used in the aero–space industry is glass fiber embedded in resin (usually epoxy matrix). This material has been used in airframes since the 1950s (Boeing 707), where the complete struc–ture contained 2% of composites. Nowadays, this number is much higher and goes to more than 50 % on modern designs like Boeing 787 (50% composites, 20% alumi–num, 15 % titanium, 10% steel, and 5% other materials). Apart from glass-based composites, carbon fiber embed–

ded in the epoxy matrix is another popular and very efficient composition used in aerospace. As an example, the modern Airbus 350 is manufactured, con–taining 53% carbon-composite, which resulted in a 25% reduction in operating costs, fuel burn, and CO_2 emissions.
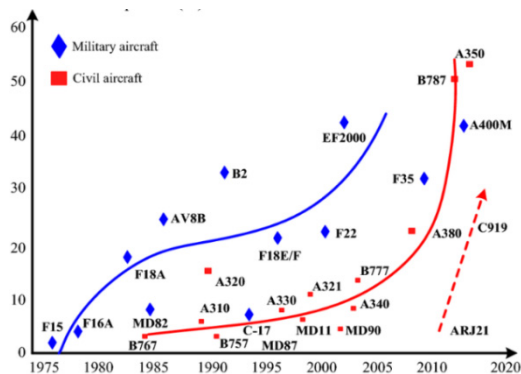

Figure 1 Application of composites on military and civil aircraft [1]

Analyzing the data presented in Figure 1 and given in [1], it undoubtedly can be concluded that the application of composite systems on airframes is on the rise when modern designs are in question. Based on the same data, another intriguing point is worth investigating. At the beginning of the application of composites in the aerospace industry, military aircraft contained a much higher percentage of composites compared to civil aircraft. In the modern era, this has changed. Based on the data presented in [1], it can be concluded that civil aircraft, in terms of a composite application, precede military applications. Furthermore, the steep gradient of composite applications in civil aircraft applications is evident, especially in the new millennium. Hence, it is worth analyzing these materials in the realm of stability of plates and shells investigated in this paper.

In the conclusion of the introductory part, it is worth mentioning new, emerging, and fabrication techniques. A group of fabrication techniques where parts are fabricated in a layer-wise manner from digital files (usually directly obtained as input from a variety of CAD systems or 3D object scanners) is referred to as additive manufacturing. Instead of milling a workpiece from a solid block, additive manufacturing builds the part layer-by-layer from the material supplied. In recent years, additive manufacturing techniques have constantly been improving and are the research focus of many companies' researchers and OEMs. The introduction of additive manufacturing technology has impacted many manufacturing processes since many designs can now be simplified and the prototyping timelines considerably shortened. On the other hand, the application of additive manufacturing techniques has changed the way parts are assembled, and complex part design has been greatly simplified.

In recent years, additive production technologies have improved significantly, increasing the possibility that 3D-printed mechanical systems elements will be transferred from research areas into manufacturing and production processes. The aerospace industry was one of the first to implement additive manufacturing in the design and production process.

A variety of different polymers are available in filament form and are suitable for 3D printing. For general use, the most popular polymers are Polylactic acid (PLA), Acrylonitrile butadiene styrene (ABS), Polyethylene terephthalate (PET), Nylon, Thermoplastic elastomer (TPE), and Polycarbonate. For more advanced use, also available in filament form are PLA/Carbon blend, Polypropylene, Acetal, Polymethyl methacrylate (PMMA), and Fluorene Polyester (FPE).

PLA represents one of the most popular 3D printing materials, mostly because of its availability, price, ease of handling, and relatively good characteristics. For most extrusion-based 3D printers, PLA is the standard filament of choice because it requires low temperatures and does not require a heated bed. Furthermore, PLA is inexpensive, and manufactured parts can be used for a wide variety of industrial applications. From an ecological point of view, PLA is one of the most environmentally friendly materials on the market. The advantages of PLA are low cost, stiffness, relatively good strength, good dimensional accuracy, and good shelf life, whereas disadvantages can be summarized as low heat resistance, the need for cooling fans during manufacture, the filament can get brittle and break, and UV sensitivity.

Over the last few years, especially in the prototyping phase of drone design, unmanned aerial vehicles, and unmanned aircraft systems design and prototype manufacture, fused deposition modeling techniques based on thermoplastic filament material have been very often used. Many researchers have focused in recent years on determining the physical and mechanical properties of FDM-manufactured parts of flying vehicles, as well as their respective tensile strengths and failure modes. In this paper, the aeroelastic stability of tapered PLA and thin composite plates exposed to axial subsonic flow is analyzed. Plates are created using 3D printing technology and PLA filament.

2. ANALYSIS MODEL

In this section, and bearing in mind the objective to determine the effect of the aspect and taper ratio, of plates and shells, on their stability, known models for torsional divergence, flutter, and missile stability are used. These models used in the analysis in this work are modified, in that respect, to take into account the orthotropic material properties based on the existing and accepted theories primarily for composite structures. To estimate the impact of the geometry and change of the plate, resulting in aspect and taper ratio change, on plate stability, a set of equations is used, which are presented in the following text.

2.1 Dynamic aeroelastic equations for flutter

Flutter represents a very complex phenomenon. From the point of flutter speed estimate, throughout history, many modeling approaches have been attempted. As it was mentioned in the earlier text, it has been investigated since the early days of flight. At that time, many flutter speed equations had been developed. As an example, Kussner (1929.) found that for lifting surface flutter occurs when:

$$k_{cr} = \frac{\omega \cdot c}{2 \cdot U} = 0.9 \text{ to } 0.12 \quad (1)$$

Equation (1) represents the well-known Kussner's formula, where ω represents the fundamental frequency of oscillations of a lifting surface in torsional oscillations in still air, U is flow mean speed, and c is chord length. The practical use of the presented equation can be interpreted in the following way: To prevent flutter from occurring, the reduced frequency should be significantly higher than k_{cr} value (equation 1). Based on that, Kushner's flutter criterion reads:

$$U_{cr} = \frac{\omega \cdot c}{2 k_{cr}} \quad (2)$$

In equation 2 U_{cr} represents the critical flutter speed, expressed in terms of fundamental torsional frequency, critical value k_{cr} computed from equation 1 and lifting surface chord.

Another approach, suggested by R.H Ricketts [2]at the National Aeronautics and Space Administration agency, suggests that against the flutter following relation must be satisfied:

$$FSI = \frac{V_F}{\left(b \cdot \omega \cdot \sqrt{\mu}\right)} \quad (3)$$

In this relation, where V_F is the flutter speed, b is the length of the semi-chord at the three-quarters, ωisthe natural frequency (radians per second) of the torsion mode, and μ is the ratio of the wing weight to the weight of the volume of air in a frustum of a cone enclosing the wing. The "three–quarter" semi-chord span is a known approach in aeroelastic analysis, and it is referred to as the "typical section approach"[3-6]. It is recommended that FSI is approximately equal to one-half at all altitudes of flight.

Based on a binary model (2 DOF, plunging h and twisting θ), depicted in Figure2, the flutter velocity V_F can be expressed using equation 4. A detailed explanation of this flutter model is given in[7].
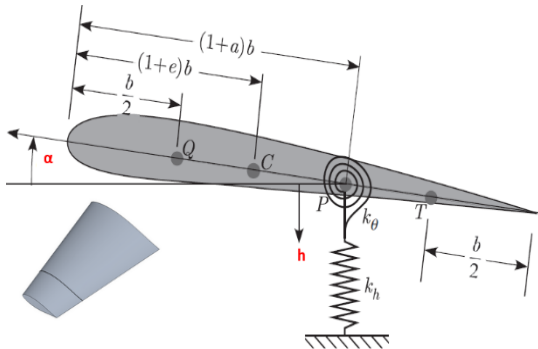

Figure 2. Flutter binary model

For the presented system of 2 DOF, using energy principles, in order to derive the equations of motion, expressions for kinetic and potential energy, in terms of plunge and twist degrees of freedom, with the artificial damping term (D)can be expressed in the following form:

$$E_k = \frac{1}{2}\left(\int_l dm\right)\dot{h}^2 + \frac{1}{2}\left(\int_l r dm\right)2\dot{h}\dot{\alpha} + \frac{1}{2}\left(\int_l r^2 dm\right)\dot{\alpha}^2$$

$$E_p = \frac{1}{2}C_h \cdot h^2 + \frac{1}{2}C_\alpha \cdot \alpha^2 \quad (4)$$

$$D = \frac{1}{2}\frac{g_h C_h \dot{h}^2}{\omega} + \frac{1}{2}\frac{g_\alpha C_\alpha \dot{\alpha}^2}{\omega}$$

Using the Lagranges principle leads to the equations of motions of the presented system:

$$\ddot{h} + \frac{S_k}{M_k}\ddot{\alpha} + g_h \frac{\omega_h^2}{\omega}\dot{h} + \omega_h^2 h = -\frac{R_z(t)}{M_k}$$

$$\ddot{\alpha} + \frac{S_k}{I_k}\ddot{h} + g_\alpha \frac{\omega_\alpha^2}{\omega}\dot{\alpha} + \omega_\alpha^2 \alpha = \frac{M_T(t)}{I_k} \quad (5)$$

In the previous relation, $Rz(t)$ and $M_T(t)$ are aerodynamic forces and moments consecutively, with artificial damping for structural and fluid damping included and denoted as g_h and g_α, respectively. The natural frequencies (modes) of the system analyzed are given as ω_h (bending) and ω_α. (twist). Inertial characteristics of the lift surface section (Figure 2, moments of inertia) are I_k and S_k.

For the Quasi-steady flows, aerodynamic force is presented in the following form:

$$R_z(t) = -\frac{1}{2}C_{L\alpha} \cdot \alpha(t) \cdot \rho \cdot V_0^2 \cdot c \quad (6)$$

Based on this model, the flutter velocity, in terms of natural frequencies, flight conditions, and geometric surface parameters, is expressed:

$$V_F = U(\omega_\alpha = \omega_h) = \sqrt{\frac{\pi c^2 r_\alpha^2 \mu \left(\omega_\alpha^2 - \omega_h^2\right)}{8 C_{L\alpha} x_a}} \quad (7)$$

Frequencies, ω_h, and ω_α are the bending and twisting natural frequencies of the plate, r_α is the radius of gyration about the mid-chord, and μ is the dimen–sionless plate airstream mass ratio. The lift coefficient is denoted as $C_{L\alpha}$, which depends on the airfoil shape and the angle of attack α with the included condition that flutter (stability loss) occurs when bending and twisting frequencies coalesce, or in mathematical form:

$$(\omega_\alpha = \omega_h) \quad (8)$$

The unsteady solution of equation (5) is obtained by using one of the unsteady subsonic theories where the aerodynamic force and aerodynamic moment are expre–ssed in the following form:

$$R_z(t) = \pi\rho\frac{l}{2}V^2\left\{\begin{array}{l}\frac{l}{2V^2}\ddot{h} + \frac{2}{V}C(k)\dot{h} - \frac{l^2 a}{4V^2}\ddot{\alpha} + \\ +\left[1+(1-2a)C(k)\right]\frac{l}{2V}\dot{\alpha} + 2C(k)\alpha\end{array}\right\} \quad (9)$$

$$M_T(t) = -\pi\rho\frac{l^2 V^2}{4}\left\{-\frac{al}{2V^2}\ddot{h} - (1+2a)\frac{1}{V}C(k)\dot{h} + \left(\frac{1}{8}+a^2\right)\frac{l^2}{4V^2}\ddot{\alpha}\right\}$$
$$-\pi\rho\frac{l^2 V^2}{4}\left\{-\left[a-\frac{1}{2}+2\left(\frac{1}{4}-a^2\right)C(k)\right]\frac{l}{2C(k)}\dot{\alpha} - \right.$$
$$\left. -(1+2a)C(k)\alpha\right\}$$

In the previous equation, the value of circular function $C(k)$ is given using the following relation and as a function of reduced frequency denoted as k:

$$C(k) = \frac{(1+i10.6k)\cdot(1+i1.774k)}{(1+i13.51k)\cdot(1+i2.745k)} \tag{10}$$

In this paper, another flutter model used to estimate taper and aspect ratios of plates and shells on the overall stability is proposed by the National advisory committee for aeronautics. This is presented in technical note No 4197. Based on this, flutter boundary velocity for lifting surfaces is defined in the following form.

$$\left(\frac{V_F}{a}\right)^2 = \frac{G}{\dfrac{39.3\cdot A^3}{\left(\dfrac{t}{c}\right)^3\cdot(A+2)}\left(\dfrac{\lambda+1}{2}\right)\cdot\left(\dfrac{p}{p_0}\right)} \tag{11}$$

In this relation, V_F is flutter speed, a is the speed of sound at flight altitude, G is the material shear modulus of elasticity, t is plate thickness, p/p_0 is the ratio of the pressure to standard pressure, and A and λ are aspect and taper ratios.

The modern approach to flutter speed predictions requires a numerical approach, and algorithms are very well established. This is known as Computational Flutter Analysis (CFA). The basis of this approach relies on the application of known K, P-K, and PKNL algorithms[8-10]. Many commercial software modules implemented these algorithms, like ZONA aero and Nastran. The CFA procedure requires the construction of a structural model, which is by splines connected to the aerodynamic model. The unsteady aerodynamics models are generally used. From the aerodynamics model, loads are transferred to the structure using the spline model), which is flexible, and hence since the deformed structure changes the load, the newly deformed structure with the corresponding changed load is analyzed at every iteration as elastic. In the CFA approach, the flutter is assumed to occur when the structural damping is zero. Based on the research reported in [7], it was found that this approach is the most accurate and renders the result very close to experimentally obtained in wind tunnel tests performed for subsonic flows. However, the CFA approach is tedious, time-consuming, and requires very high CPU resources. In this research, the CFA approach is used for results verification of previously mentioned models, especially for the plates with low to moderate aspect and taper ratios.

2.2 Torsional Divergence Model

Taking into account the mutual effects of elastic and aerodynamic forces, static aeroelastic phenomena known as divergence are investigated in this section. Lifting surface torsional divergence is the most common divergence phenomenon that occurs when the lift surface e local angle of twist increases (rotates) to the point where structural failure is certain due to increased stress beyond allowable stress limits (material constraints). This arises when the aerodynamic lifting forces on a structure generate a moment that twists the lift surface about its shear centers. As a result of this twisting action, the local angle of attack is increased. With the increased angle of attack, more lift is generated, which in turn produces more twists. At a certain point, the aerodynamic forces and the elastic forces will reach equilibrium, or the elastic forces will not be capable of sustaining this increase, and hence the failure of the structure is definite. The speed at which described phenomena is exhibited (failure point) is referred to as divergence speed.

As in dynamic aeroelasticity, several models exist for divergence speed estimates and can be found in the literature [11-13]. Furthermore, apart from theoretical approaches (such as the "typical section method"), divergence speed can be determined experimentally or by a combination of analytical and numerical models described in the following text. The model used in this research is depicted in Figure 3:
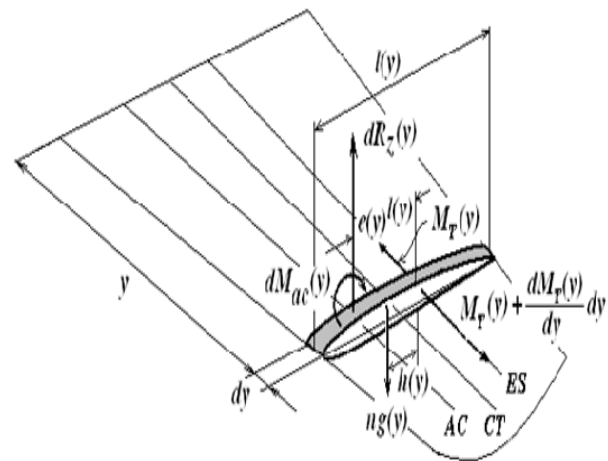
Figure 3. Torsional divergence model

$$\left[GJ(y)\right]\cdot\frac{d^2\theta}{dy^2}+\left[\frac{d}{dy}\left(GJ(y)\right)\right]\cdot\frac{d\theta}{dy}+$$
$$+\left[\frac{1}{2}\rho V^2\cdot\frac{dC_z(y)}{d\alpha}\cdot l^2(y)\cdot e(y)\right]\cdot\theta \tag{12}$$
$$=-\frac{1}{2}\rho V^2\frac{dC_z(y)}{d\alpha}\cdot\alpha(y)\cdot l^2(y)\cdot e(y)-$$
$$-\frac{1}{2}\rho V^2 C_{mac}(y)\cdot l^2(y)+n\cdot g(y)\cdot h(y)$$

The solution to the above divergence equation in this research is regarded as follows:

The differential equation for the equilibrium condition of the differential fin element about the shear center, presented for convenience, can be expressed as:

$$F(y)\cdot\frac{d^2\theta}{dy^2}+F'(y)\cdot\frac{d\theta}{dy}+$$
$$+A(y,V)\cdot\theta = B(y,V) \tag{13}$$

Where by comparison, one may conclude that in the previous equation, variable coefficients are:

$$F(y) = GJ(y), \quad F'(y) = \frac{d}{dy}(GJ(y))$$

$$A(y,V) = \left[\frac{1}{2}\rho V^2 \cdot \frac{dC_z(y)}{d\alpha} \cdot l^2(y) \cdot e(y) \right] \quad (14)$$

$$B(y,V) = -\frac{1}{2}\rho V^2 \frac{dC_z(y)}{d\alpha} \cdot \alpha(y) \cdot l^2(y) \cdot e(y) - $$
$$-\frac{1}{2}\rho V^2 C_{mac}(y) \cdot l^2(y) + n \cdot g(y) \cdot h(y)$$

Assuming the solution in the form:

$$\theta(y) = \sum_{i=1}^{N} a_i \cdot \varphi_i(y) \quad (15)$$

And functions $\varphi_i(y)$ are chosen to satisfy initial conditions:

$$\varphi_i(0) = 0, \quad \varphi_i'(b/2) = 0 \quad (16)$$

Using Galerkin's method [14-15] for error minimization of the assumed solution for the differential equation (eq. 8), it follows:

$$\sum_{i=1}^{N} a_i \cdot \int_0^{b/2} \left[F(y)\varphi_i''(y) + F'(y)\varphi_i'(y) + A(y,V)\varphi_i(y) \right]$$
$$\cdot \varphi_j(y) \cdot dy = \int_0^{b/2} B(y,V) \cdot \varphi_j(y) \cdot dy \quad (17)$$

Theoretically, torsional divergence when:

$$\theta(y, V_D) \to +\infty \quad (18)$$

Which can be regarded as a divergence condition. Using this approach, the analysis assumes the flight speed (within the flight vehicle flight envelope), and using a numerical approach solves the divergence equation for the guessed estimated speed, which is usually done by incrementing the speed values. The lifting surface and sectional rotational field are obtained (Figure 6.). With the speed increase, it is expected that the surface section rotations increase as well. The speed at which the divergence condition is met and section rotation approaches infinity is considered divergence speed (V_D)

For further reference, Table 2 contains applicable formulas for torsional constant calculations (required in differential divergence equation) for typical lifting surface designs (two spar wings (A), airfoil cross-section (B), and flat plate surface (B)).

In the case of two spar wings, for calculating the cross-sectional torsional constant J, the analyst, with great accuracy (within 6%), can include spar walls and top and bottom skins. The formula for that particular case and with this approximation is given in Table 2, section A. This concept is presented in Figure 4.

For the lifting surfaces, designed as a solid in a shape of an airfoil, a sectional torsional constant can be calculated using the formula given in Table 2, section B. It is worth noting that mentioned formula renders

approximate values for this type of cross-section, whereas more accurate results can be obtained using relations based on the Theory of elasticity. The formula stated in Table 2, section B is derived based on the approximation that the airfoil shape (valid for thin airfoil) is approximated by the elliptic relation:
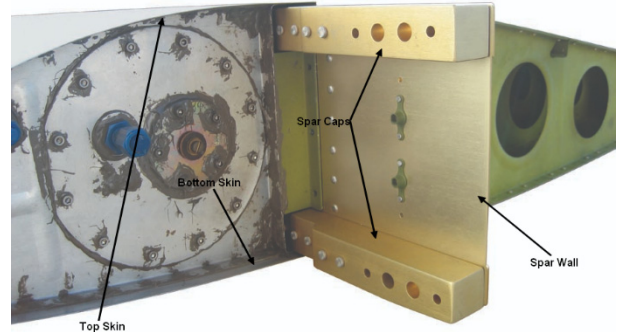
Figure 4. Wing-spar, calculation of torsional constant / per section using formula in Table 2.

$$b(y) = b \cdot \left[1 - \left(\frac{4y^2}{a^2} \right) \right] \quad (19)$$

Solution of the integral for torsional constant J in the form:

$$J = \frac{1}{3} \cdot \int_{-a/2}^{a/2} b^3(y)dy \quad (20)$$

In previous relations, y denotes the lift surface variable span coordinate, b is the maximum thickness of the airfoil a is the chord length. The solution of the integral (19) leads to the airfoil section (approximated) torsional constant.
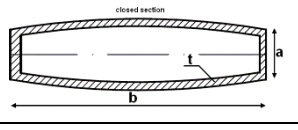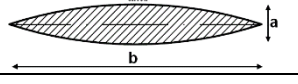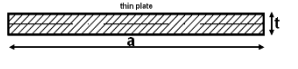
For the flat plate cross-section (theoretical lift gradient of 2π/rad), the torsional constant formula is given in Table 2, section C, and also represents the approximate expression, with an acceptable degree of accuracy in the analysis of lifting surface torsional divergence problems.

Based on what was previously said and based on the model presented, using Galerkin's approach, it is possible to obtain the rotational displacement field of the lifting surface for typical air-worthy designs. It is always convenient to present the results in a graphical form, as presented in Figure 6. On the ordinate, the value of section rotation is given, and section location (measured from the root, clamp) is given on the abscissa. This graph, as presented, is given for the guess-estimated flight speed within the flight envelope; analyzing the condition given by the relation (17), it can be concluded that this is a theoretical value of divergence speed, where in practice, the failure of the structure is expected to occur before

Once the rotational field has been calculated, using the sectional rotations, and in order to obtain more realistic values for divergence speeds for a particular configuration and take into account material properties and stresses developed in the loaded structure, a finite element model of the structure analyzed can be created where the boundary conditions can be created from the

rotational displacement field previously calculated. The rotational displacement field (known) is recalculated to linear section vertical displacements (Figure 5) and imposed at the locations (corresponding location spanwise) of the lifting surface.

Table 1 torsional constants formulas for typical cross-sections

A	closed section (b, a, t)	$J = \dfrac{4A^2}{\oint_c \dfrac{ds}{t}}$
B	airfoil (b, a)	$J \approx \dfrac{16a^3 b}{105}$
C	thin plate (a, t)	$J \approx at^3 \cdot \left(\dfrac{1}{3} - 0.21\dfrac{t}{a}\right)$ $\cdot \left(1 - \dfrac{t^4}{12a^4}\right)$

Figure 5. Sectional rotational field

Assuming small rotations, the angle θ is approximately equal to the tangent of the angle, which is equal to the sum of the displacements, Δl and Δ2, divided by the chord distance apart (Figure 6).
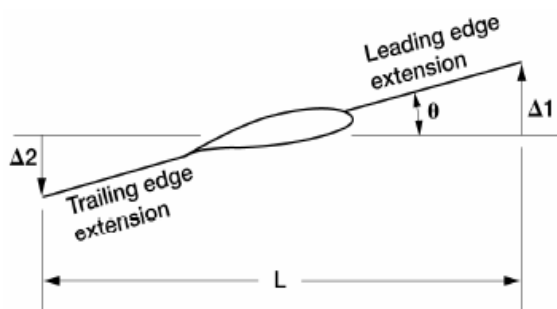
Figure 6. Sectional rotational field

At the lifting surface, selected chords previously calculated displacements of leading and trailing edges are imposed as boundary conditions (enforced displacement), as it is shown in Figure 7.

Based on this model stress-strain field can be calculated, which renders the information about stress magnitude in the loaded structure as a function of the flight speed.
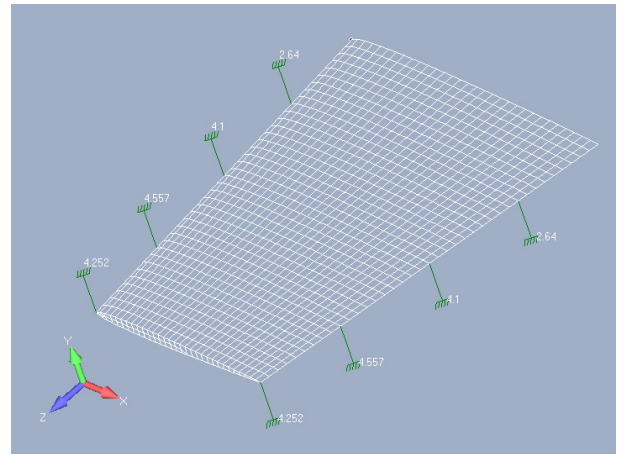
Figure 7. Section rotational displacement field boundary condition (solid airfoil cross-section)

Theoretical divergence speed criteria, given in relation (18), can be transformed to include stress cri–terion or strain criterion.

$$\theta(y, V_D) \le \begin{bmatrix} \sigma_{\max},\ \tau_{\max} \\ \varepsilon_{\max},\ \gamma_{\max} \end{bmatrix} \qquad (21)$$

Maximal stress and strain values in relation (21) are materially constrained, whereas the displacement field is governed by overall flight vehicle design (lifting or control surface deformation).

Torsional divergence speed, based on the "typical section" approach, assumes that the divergence will occur when the following is satisfied:

$$V_D = \sqrt{\frac{2 \cdot C_{\theta\theta}}{\rho \cdot \dfrac{dC_z}{d\alpha} \cdot S \cdot e \cdot l}} \qquad (22)$$

In the previous relation, the term $C_{\theta\theta}$ is the torsional stiffness of the structure usually obtained by experi–mentation. The structure is loaded with the known twis–ting moment, and the displacement of the leading and trailing edges is measured. Based on the twisting rela–tion, the stiffness can be calculated. The schematics of the torsion fixture applicable for this test are given in Figure 8.
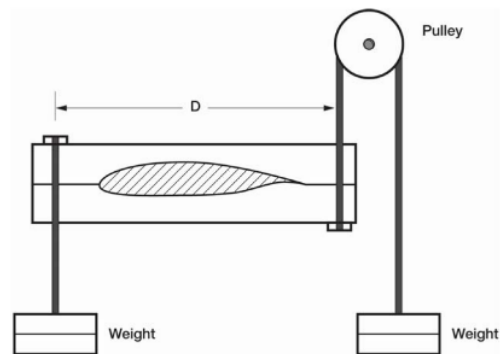
Figure 8. Loading fixture for applying moments

2.3 Material Model

As can be seen from the analysis of existing flutter models and computational approaches in the previous

section, material characteristics play an important role in aeroelastic analysis (static and dynamic). On the other hand, composite materials manufactured in the form of plates and shells are of particular interest and, as was seen previously, are often used in airframe construction.

In any structural problem, Generalized Hooke's law is used. Stresses to strains are related through a stiffness matrix whose elements are elastic coefficients depen–dent on material characteristics and usually obtained by experimentation.

In composite analysis terms, the ABD matrix is often used. The 6x6 matrix known as ABDserves as a relation between the applied loads and the associated strains in the laminate. It defines the elastic properties of the laminate [16-17]. Submatrix B in the ABD laminate matrix is the coupling term between axial and shear components. It is possible to produce laminate in such a way that the B submatrix is zero; hence in these laminates, the above-mentioned coupling does not exist. This is the case with symmetric and quasi-isotropic (QI) lay-ups. Symmetric laminates are laminates where lay-up is symmetric with respect to the neutral surface. This symmetry condition must be satisfied for both geometry and material properties. Several typical symmetric laminate lay-ups are presented in Figure 3.
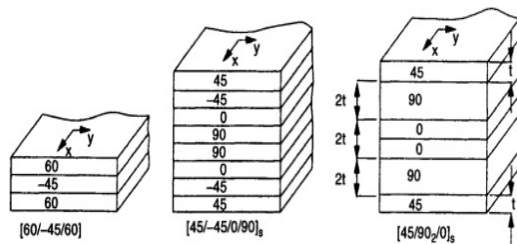
Figure 9. Flutter binary model

Quasi-isotropic (QI)is of great interest in the initial phases of the design. A quasi-isotropic laminate is attained when the laminas are oriented in such a way as to produce an isotropic [A] submatrix. The coefficients $A_{16} = A_{26} = 0$, and the extension and shear are unco–upled. In this lay-up, the components of [A] are inde–pendent of laminate orientation, and for the quasi-iso–tropic laminate, the stack-up must satisfy the following relation:

$$\left[0^0 / \frac{180^0}{m} ... (m-1)\frac{180^0}{m} \right]_{ns} \qquad (23)$$

Number m represents the number of different orientations in the laminate and is the number of repetition sequences. This stack-up lamina combination excludes coupling effects. Composite (in-plane) stiff–ness is independent of composite orientation, which is the main reason why this type of stack-up is often used as the starting point, bearing in mind the great number of variables (fiber type, matrix type, volume fractions, fiber orientation…) when designing with composites.

This is one of the reasons why this stack-up is considered in the preliminary stages of design and is further improved to achieve the optimum[18-19]. The optimal design for composite airframes is usually done using a numerical approach, and at present days several optimization algorithms have been implemented into software modules, Hypersizer software developed by NASA being one of them. The objective function is usually mass reduction obtained by fiber orientation rearrangement and lamina thickness optimization.

Following the works of Akkerman et al., for QI laminates[20], the in-plane (x-y shear plane) shear modulus of QI laminates is expressed in the following form:

$$G_{xy} = \frac{1}{2} \cdot G_{12} + \frac{1}{8} \frac{E_1 \cdot \left(E_1 + E_2 - 2\upsilon_{12} E_2 \right)}{E_1 - 2\upsilon_{12}^2 E_2} \qquad (24)$$

In the equation for shear modulus, Youngs' moduli (E_1, E_2) and Poisson ratio (v_{12}) can be obtained using composite micromechanics theories [6], provided that the mechanical characteristics of composite phases (fi–bers, matrix, and void content) are known, and are usually obtained from the original component manufac–turer. In this paper, the Akkerman equation for QI laminates is used for flutter velocities predictions for flutter velocities in cases where the NACA boundary equ–ation (equation 4) is used for analysis.

For typical lamina, with respect to fiber volume fraction, values for essential elastic coefficients for carbon/epoxy, glass/epoxy, and PLA are given in Table 2. for reference.

Table 2: Typical lamina properties for different systems

	ρ [g/cm^3]	d [μm]	V_f [-]	E_1 [GPa]	E_2 [GPa]	G_{12} [GPa]	v_{12} [GPa]
E-Glass / Epoxy	2.10	16	0.55	39	8.6	3.8	0.28
Carbon / Epoxy	1.58	6.5	0.63	142	10.3	7.2	0.27
PLA	1.24	(Raster dep.)	(3D Print)	4.4	4.4	(Calculated)	0.3

2.4 Modal Analysis

The determination of modal frequencies required in all dynamic aeroelastic analyses can be determined by experimentation, analytics analysis, and numerical analyses. In this research, both analytic and numerical approach is deployed, followed by experimental verification.

First, considering the thin plates and shells analyzed, from the stability of view, the Rayleigh-Ritz approach is used. It is considered that the plate analyzed is cantilevered. This can be regarded as a wing attached to a fuselage or a fin to a missile body. According to Rayleigh-Ritz theory, for a cantilevered beam, fundamental frequencies of oscillations are given in the following form[14]:

$$\omega_n = \frac{\lambda_n}{b^2} \sqrt{\frac{D}{\rho \cdot t}} \qquad (25)$$

In this relation,n represents the mode number of oscillation, and Coefficients λ_n are the function of

boundary condition, material type, and analyzed plate taper ratio. Coefficients λ_n for the first two modes (bending and twisting) for isotropic materials as a function of taper ratio (tip chord/root chord) are given in Table3.

Table 3: Isotropic material Coefficients

C_{tip} / C_{root}	Mode 1 λ	Mode 2 λ
2	3.51	5.37
1	3.49	8.55
0.5	3.47	14.90

In order to adequately apply Rayleigh-Ritz theory for orthotropic materials (composites), recalculation of coefficients is required. In this analysis, and bearing in mind composites as a building block of airframes, by performing FEA (finite element analysis - modal) for carbon-based and E-glass-based composite systems, and cantilevered components λ_n coefficients required in the previous equation can be obtained from the following equations:

$$\lambda_1 = 0.0257 \cdot A + 3.46$$
$$\lambda_2 = 8.8113 \cdot A^{0.736} \qquad (26)$$

In equation (25) ρ is the material density, and D is plate flexural rigidity computed from the following relation:

$$D = \frac{E_{eq} \cdot t^3}{12\left(1 - v_{eq}^2\right)} \qquad (27)$$

In the previous relation, E_{Eq} represents the Equi–valent modulus of elasticity(Young's modulus of elasticity.), and D is plate rigidity. The same applies to Poisson's ratio in the same equation. As QI laminates of primer interest in this research, the equivalent modulus of elasticity can be calculated from the isotropic relation:

$$E_{eq} = 2 \cdot \left(1 + v_{xy}\right) \cdot G_{xy} \qquad (28)$$

The shear modulus required by the previous relationship can be calculated using equation 7, whereas Poisson's ratio is set to 0.3 for the preliminary analysis.

3. RESULTS AND DISCUSSION

Based on the models presented in the previous text, static stability and dynamic stability of tapered are analyzed for the different taper and aspect ratios [21-22]. The taper ratio was varied from a starting value of 0.5 to a value of 1 (square plate). The aspect ratio analyzed was from 0.5 to 2. For all geometries analyzed, results are presented in Table 4.

Based on the results obtained for flutter velocities using the NACA boundary equation and unsteady flutter model presented in the previous section, it was found that the Naca boundary equation gives better results for low aspect ratios, whereas for moderate to high aspect ratios, unsteady flutter equation renders results closer to experimentally obtained velocities in a subsonic wind tunnel [7]. The original flutter boundary equation used to estimate the flutter velocities for low aspect ratios and for orthotropic structures (composites) was modi–fied in that respect, that elastic coefficients (material shear modulus) are calculated based on the relation (7) and incorporated in the original equation. The modified equation is given in the following form:

$$V_f = a \cdot \left[\frac{\dfrac{(A+2)}{78.6 \cdot A^3} \cdot \left(\dfrac{t}{\dfrac{2}{S} \cdot \int_0^{b/2} c(y) \cdot dy} \right)^3 \cdot}{\dfrac{\left(G_{12} + \dfrac{1}{4} \dfrac{E_1 \cdot (E_1 + E_2 - 2v_{12}E_2)}{E_1 - 2v_{12}^2 E_2} \right)}{\left(\dfrac{c_t / c_r + 1}{2} \right) \cdot \left(\dfrac{p}{p_0} \right)}} \right]^{1/2} \qquad (29)$$

It is worth noting that this equation used in the orthotropic form (valid for QI lay-up), is also without change applicable to isotropic materials (metals) since for these types of materials, Young's moduli are equivalent ($E_1 = E_2$) and all material isotropic relations are valid. For orthotropic materials, the required elastic coefficients can be obtained based on Micromechanics theories, provided that the phase's mechanical data is available. These are usually obtained either from the literature or from the components manufacturer.

Dynamic stability for different geometries analyzed and expressed through flutter velocities is presented in the following figures:
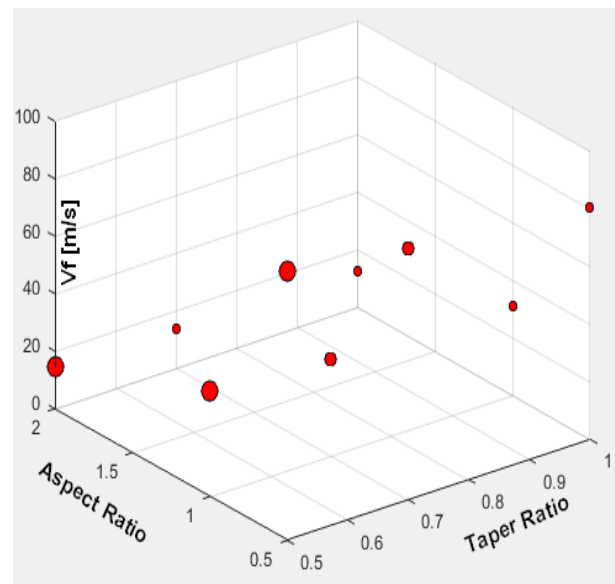
Figure 10. Flutter velocity as a function of Aspect and Taper Ratio

Analyzing the results obtained, it was observed that increasing the aspect ratio lowers the flutter velocities; however, it increases overall stability. For lower to moderate Aspect ratios, the taper ratio does not significantly influence flutter speeds (Figure 11). For low ratios, flutter speeds are the maximum for a particular configuration. Flutter models used render similar results for moderate ratios.
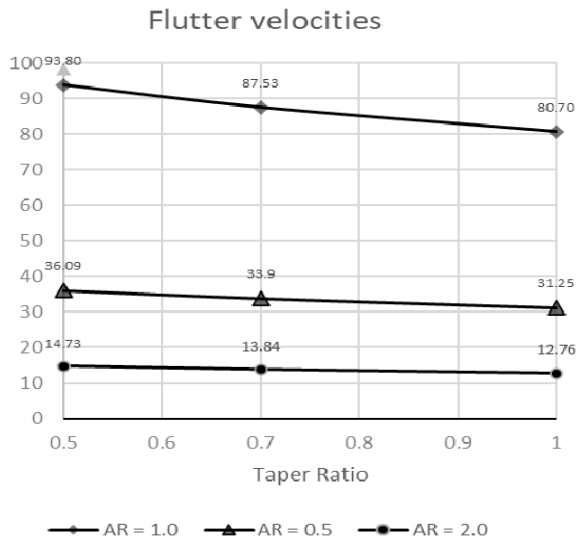
Figure11. Flutter velocity as a function of Taper Ratio

Using the CFA approach for maximum and mini–mum ratios, a complete numerical analysis of the flutter speeds is performed using MSC Flight-loads commer–cial software. For the three configurations analyzed, results are presented in tables 4-6.

Based on CFA, for a particular mode (twisting or bending), the value of structural damping is analyzed. For a frequency of oscillation where the damping term turns positive (no damping in a structure), the corres–ponding velocity is considered a velocity at which the loss of stability occurs. Analyzing all modes of oscil–lation, the minimal value for velocity where damping is positive is considered to be the velocity at which the loss of stability will occur. This value is further compared to envelope data and applicable standards.

In all analyses performed in this study, the thickness is kept constant. There is no doubt that the thickness highly affects the flutter speed. With the increase in thickness, the flutter speed increase. Detailed analysis of thickness effects on flutter speed is given in [4].

The divergence speeds have been calculated for dif–ferent geometries given in Table 4. The methodology used for divergence calculation is described in the previous text.

For particular configuration values for a torsional contant (J) have been calculated for a number of sections along the span (for a particular chord length at that location) and then used to approximate the $J(y)$, where y is the span, with a Second-Degree Polynomial Function.

It was found that torsional divergence speeds are higher, compared to flutter speeds, for the same struc–tural configuration. However, they have to be calculated since they give a good insight into the overall structure stiffness and are required by many standards currently in use.

The overall stability is estimated for all confi–gurations analyzed. The aerodynamic characteristics considered are the normal force coefficient derivative, the center of pressure, the roll forcing moment coef–ficient derivative, the roll damping moment coefficient derivative, the pitch damping moment coefficient derivative, and the drag coefficient. For a typical confi–guration and for varying different geometries of the stabilizing surfaces (geometries with respective dimen–sions are presented in Table 4), results for the drag coefficient (Cx) and Stability coefficient as functions of aspect and taper ratios are presented in Figure 12 and Figure 13.

It can be seen that the increase in aspect ratio inc–reases the stability coefficient; however, with the inc–rease of aspect and taper ratio drag coefficient increases (Table 4.). Results for drag coefficient, as a function of aspect and taper ratios, are given in Fig. 13.
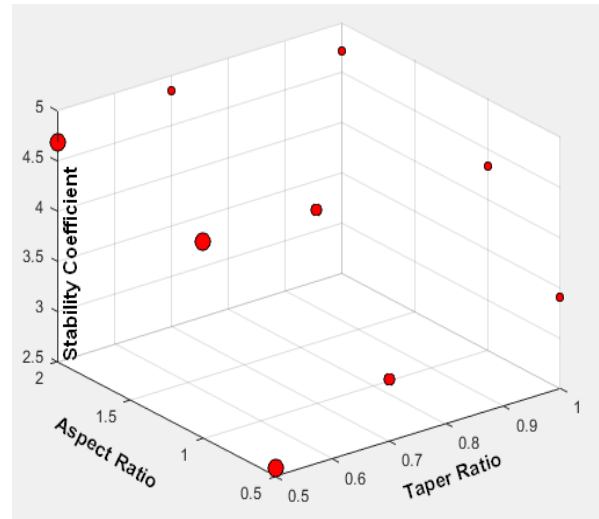
Figure 12. Stability coefficient as a function of taper and aspect ratios
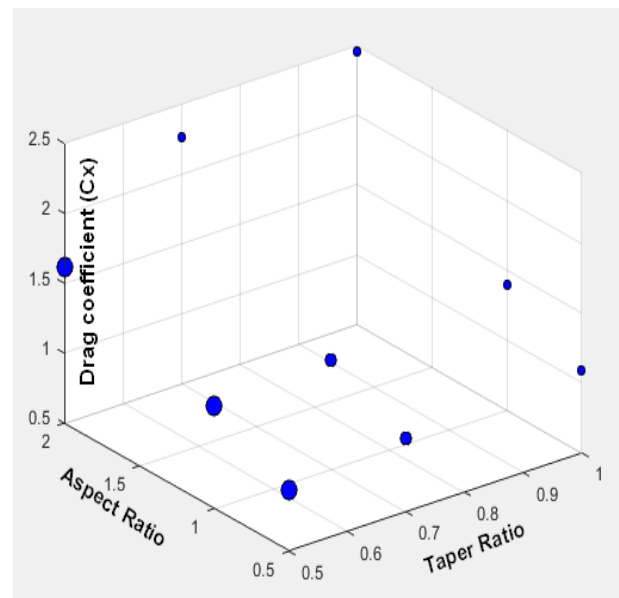
Figure 13. Drag coefficient as a function of taper and aspect ratios

The effect of material on flutter speeds for E-glass / Epoxy and Carbon /Epoxy is analyzed. Results are pre–sented in Figure 14 in the form of a V-g diagram (speed versus damping). Material stiffness directly influences the flutter speeds. In composites, also the lay-up has a great impact on the speed. This needs further investi–gation.

Table 4 Results Summary
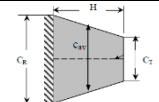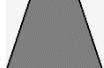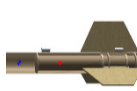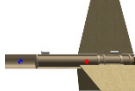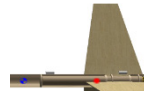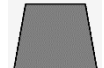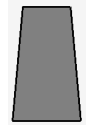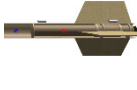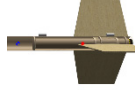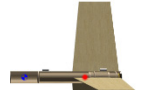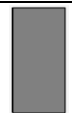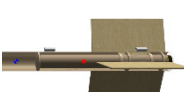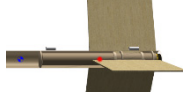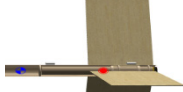
	AR= 0.5	AR= 1	AR= 2
λ= 0.5	Model 1	Model 2	Model 3
	H = 67.5 [mm]	H =135 [mm]	H = 270 [mm]
	C_R = 180 [mm]	C_R = 180 [mm]	C_R = 180 [mm]
	C_T = 90 mm	C_T = 90 mm	C_T = 90 mm
	Cav = 140 [mm]	C_{av} = 140 [mm]	C_{av} = 140 [mm]
	Stability 2.59 [cal]	Stability 4.46 [cal]	Stability 4.69 [cal]
	C_x = 0.94 [-]	C_x = 1.23 [-]	C_x = 1.61 [-]
	V_F =93.8 [m/s]	V_F =36.9 [m/s]	V_f =14.73 [m/s]
	Δ =127623 [rad/s]^2	Δ =49050 [rad/s]^2	Δ =10145 [rad/s]^2
λ= 0.7	Model 4	Model 5	Model 6
	H = 76.5 [mm]	H = 153 [mm]	H = 306 [mm]
	C_R = 180 [mm	C_R = 180 [mm]	C_R = 180 [mm]
	C_T = 126 [mm]	C_T = 126 [mm]	C_T = 126 [mm]
	C_{av} = 154.59 [mm]	C_{av} = 154.59 [mm]	C_{av} = 154.59 [mm]
	Stability 3.12 [cal]	Stability 4.43 [cal]	Stability 4.85 [cal]
	C_x = 1.03 [-]	C_x = 1.28 [-]	C_x = -
	V_F =87.53 [m/s]	V_F =33.9 [m/s]	V_F =13.84 [m/s]
	Δ =123125 [rad/s]^2	Δ =37572 [rad/s]^2	Δ =7506 [rad/s]^2
λ= 1	Model 7	Model 8	Model 9
	H = 90 [mm]	H = 180 [mm]	H = 360 [mm]
	C_R = 180[mm]	C_R = 180 [mm]	C_R = 180 [mm]
	C_T = 180[mm]	C_T = 180[mm]	C_T = 180[mm]
	C_{av} = 180[mm]	C_{av} =180[mm]	C_{av} =180[mm]
	Stability 3.41 [cal]	Stability 4.33[cal]	Stability 4.72 [cal]
	C_x = 1.09 [-]	C_x = 1.40 [-]	C_x = 2.45 [-]
	V_F =80.7 [m/s]	V_F =31.25 [m/s]	V_F =12.76 [m/s]
	Δ =102479 [rad/s]^2	Δ =26181 [rad/s]^2	Δ =5056 [rad/s]^2

Table 5 CFA Results for AR=λ=0.5

```
                                     FLUTTER   SUMMARY
                       CONFIGURATION = AEROSG2D    XY-SYMMETRY = ASYMMETRIC      XZ-SYMMETRY = ASYMMETRIC
          POINT =    2     METHOD = PKNL


     KFREQ         1./KFREQ      DENSITY      MACH NO.      VELOCITY       DAMPING       FREQUENCY       COMPLEX    EIGENVALUE
    5.4647       1.82993E-01   1.00000E+00   0.00000E+00   1.00000E+01   -6.31303E-03   1.24247E+02   -2.46419E+00   7.80670E+02
    3.8945       2.56772E-01   1.00000E+00   0.00000E+00   1.40000E+01   -9.82125E-03   1.23966E+02   -3.82489E+00   7.78901E+02
    3.0229       3.30806E-01   1.00000E+00   0.00000E+00   1.80000E+01   -1.32443E-02   1.23715E+02   -5.14755E+00   7.77321E+02
    2.4677       4.05231E-01   1.00000E+00   0.00000E+00   2.20000E+01   -1.65823E-02   1.23436E+02   -6.43040E+00   7.75572E+02
    2.0825       4.80184E-01   1.00000E+00   0.00000E+00   2.60000E+01   -1.98532E-02   1.23108E+02   -7.67834E+00   7.73513E+02
    1.7992       5.55811E-01   1.00000E+00   0.00000E+00   3.00000E+01   -2.30693E-02   1.22720E+02   -8.89406E+00   7.71074E+02
    1.5817       6.32239E-01   1.00000E+00   0.00000E+00   3.40000E+01   -2.62384E-02   1.22270E+02   -1.00788E+01   7.68245E+02
    1.4093       7.09593E-01   1.00000E+00   0.00000E+00   3.80000E+01   -2.93627E-02   1.21758E+02   -1.12316E+01   7.65026E+02
    1.2690       7.88007E-01   1.00000E+00   0.00000E+00   4.20000E+01   -3.24399E-02   1.21183E+02   -1.23501E+01   7.61414E+02
    1.1526       8.67626E-01   1.00000E+00   0.00000E+00   4.60000E+01   -3.54641E-02   1.20545E+02   -1.34303E+01   7.57404E+02
    1.0542       9.48606E-01   1.00000E+00   0.00000E+00   5.00000E+01   -3.84270E-02   1.19841E+02   -1.44675E+01   7.52985E+02
    0.9698       1.03112E+00   1.00000E+00   0.00000E+00   5.40000E+01   -4.13170E-02   1.19071E+02   -1.54556E+01   7.48146E+02
    0.8966       1.11536E+00   1.00000E+00   0.00000E+00   5.80000E+01   -4.41194E-02   1.18232E+02   -1.63875E+01   7.42871E+02
    0.8323       1.20155E+00   1.00000E+00   0.00000E+00   6.20000E+01   -4.68156E-02   1.17320E+02   -1.72549E+01   7.37142E+02
    0.7752       1.28993E+00   1.00000E+00   0.00000E+00   6.60000E+01   -4.93820E-02   1.16332E+02   -1.80476E+01   7.30937E+02
    0.7242       1.38077E+00   1.00000E+00   0.00000E+00   7.00000E+01   -5.17892E-02   1.15265E+02   -1.87537E+01   7.24232E+02
    0.6782       1.47439E+00   1.00000E+00   0.00000E+00   7.40000E+01   -5.39994E-02   1.14114E+02   -1.93588E+01   7.17001E+02
    0.6365       1.57116E+00   1.00000E+00   0.00000E+00   7.80000E+01   -5.59649E-02   1.12875E+02   -1.98455E+01   7.09214E+02
    0.5983       1.67147E+00   1.00000E+00   0.00000E+00   8.20000E+01   -5.76238E-02   1.11542E+02   -2.01924E+01   7.00836E+02
    0.5631       1.77586E+00   1.00000E+00   0.00000E+00   8.60000E+01   -5.88975E-02   1.10106E+02   -2.03732E+01   6.91817E+02
    0.5306       1.88483E+00   1.00000E+00   0.00000E+00   9.00000E+01   -5.96778E-02   1.08566E+02   -2.03543E+01   6.82139E+02
    0.5002       1.99907E+00   1.00000E+00   0.00000E+00   9.40000E+01   -5.98256E-02   1.06911E+02   -2.00936E+01   6.71740E+02
    0.4718       2.11940E+00   1.00000E+00   0.00000E+00   9.80000E+01   -5.91507E-02   1.05132E+02   -1.95364E+01   6.60564E+02
    0.4451       2.24677E+00   1.00000E+00   0.00000E+00   1.02000E+02   -5.73915E-02   1.03220E+02   -1.86106E+01   6.48550E+02
    0.4198       2.38233E+00   1.00000E+00   0.00000E+00   1.06000E+02   -5.41813E-02   1.01164E+02   -1.72197E+01   6.35631E+02
    0.3957       2.52747E+00   1.00000E+00   0.00000E+00   1.10000E+02   -4.89972E-02   9.89529E+01   -1.52317E+01   6.21740E+02
    0.3726       2.68381E+00   1.00000E+00   0.00000E+00   1.14000E+02   -4.10808E-02   9.65774E+01   -1.24642E+01   6.06813E+02
    0.3505       2.85317E+00   1.00000E+00   0.00000E+00   1.18000E+02   -2.93255E-02   9.40322E+01   -8.66308E+00   5.90822E+02
    0.3292       3.03732E+00   1.00000E+00   0.00000E+00   1.22000E+02   -1.21451E-02   9.13252E+01   -3.48451E+00   5.73813E+02
    0.3089       3.23733E+00   1.00000E+00   0.00000E+00   1.26000E+02    1.25583E-02   8.84923E+01    3.49129E+00   5.56014E+02
    0.2897       3.45242E+00   1.00000E+00   0.00000E+00   1.30000E+02    4.69581E-02   8.56135E+01    1.26300E+01   5.37926E+02
    0.2719       3.67846E+00   1.00000E+00   0.00000E+00   1.34000E+02    9.20013E-02   8.28249E+01    2.39389E+01   5.20404E+02
    0.2557       3.91053E+00   1.00000E+00   0.00000E+00   1.38000E+02    1.46088E-01   8.02353E+01    3.68239E+01   5.04134E+02
    0.2412       4.14623E+00   1.00000E+00   0.00000E+00   1.42000E+02    2.06026E-01   7.78676E+01    5.03998E+01   4.89257E+02
    0.2279       4.38705E+00   1.00000E+00   0.00000E+00   1.46000E+02    2.69274E-01   7.56663E+01    6.40098E+01   4.75426E+02
    0.2157       4.63660E+00   1.00000E+00   0.00000E+00   1.50000E+02    3.34783E-01   7.35552E+01    7.73619E+01   4.62161E+02
```

Table 6 CFA Results For AR=0.7 and λ=0.5

```
                                     FLUTTER   SUMMARY
                       CONFIGURATION = AEROSG2D    XY-SYMMETRY = ASYMMETRIC      XZ-SYMMETRY = ASYMMETRIC
          POINT =    2     METHOD = PKNL


     KFREQ         1./KFREQ      DENSITY      MACH NO.      VELOCITY       DAMPING       FREQUENCY       COMPLEX    EIGENVALUE
    3.9541       2.52905E-01   1.00000E+00   0.00000E+00   1.00000E+01   -1.00346E-02   8.14173E+01   -2.56665E+00   5.11560E+02
    2.8171       3.54977E-01   1.00000E+00   0.00000E+00   1.40000E+01   -1.50492E-02   8.12086E+01   -3.83941E+00   5.10249E+02
    2.1847       4.57737E-01   1.00000E+00   0.00000E+00   1.80000E+01   -1.98913E-02   8.09713E+01   -5.05993E+00   5.08758E+02
    1.7809       5.61518E-01   1.00000E+00   0.00000E+00   2.20000E+01   -2.46114E-02   8.06739E+01   -6.23763E+00   5.06889E+02
    1.5001       6.66622E-01   1.00000E+00   0.00000E+00   2.60000E+01   -2.92389E-02   8.03097E+01   -7.37698E+00   5.04601E+02
    1.2931       7.73326E-01   1.00000E+00   0.00000E+00   3.00000E+01   -3.37822E-02   7.98790E+01   -8.47755E+00   5.01895E+02
    1.1339       8.81938E-01   1.00000E+00   0.00000E+00   3.40000E+01   -3.82346E-02   7.93808E+01   -9.53501E+00   4.98764E+02
    1.0073       9.92797E-01   1.00000E+00   0.00000E+00   3.80000E+01   -4.25790E-02   7.88129E+01   -1.05425E+01   4.95196E+02
    0.9039       1.10629E+00   1.00000E+00   0.00000E+00   4.20000E+01   -4.67892E-02   7.81727E+01   -1.14908E+01   4.91173E+02
    0.8178       1.22286E+00   1.00000E+00   0.00000E+00   4.60000E+01   -5.08282E-02   7.74559E+01   -1.23683E+01   4.86670E+02
    0.7446       1.34304E+00   1.00000E+00   0.00000E+00   5.00000E+01   -5.46451E-02   7.66578E+01   -1.31600E+01   4.81655E+02
    0.6815       1.46742E+00   1.00000E+00   0.00000E+00   5.40000E+01   -5.81707E-02   7.57728E+01   -1.38474E+01   4.76094E+02
    0.6263       1.59673E+00   1.00000E+00   0.00000E+00   5.80000E+01   -6.13096E-02   7.47945E+01   -1.44062E+01   4.69948E+02
    0.5774       1.73183E+00   1.00000E+00   0.00000E+00   6.20000E+01   -6.39296E-02   7.37158E+01   -1.48051E+01   4.63170E+02
    0.5337       1.87379E+00   1.00000E+00   0.00000E+00   6.60000E+01   -6.58457E-02   7.25264E+01   -1.50028E+01   4.55697E+02
    0.4941       2.02381E+00   1.00000E+00   0.00000E+00   7.00000E+01   -6.67853E-02   7.12201E+01   -1.49429E+01   4.47489E+02
    0.4580       2.18347E+00   1.00000E+00   0.00000E+00   7.40000E+01   -6.63554E-02   6.97845E+01   -1.45474E+01   4.38469E+02
    0.4247       2.35468E+00   1.00000E+00   0.00000E+00   7.80000E+01   -6.39631E-02   6.82082E+01   -1.37062E+01   4.28565E+02
    0.3937       2.53976E+00   1.00000E+00   0.00000E+00   8.20000E+01   -5.87002E-02   6.64807E+01   -1.22598E+01   4.17710E+02
    0.3648       2.74137E+00   1.00000E+00   0.00000E+00   8.60000E+01   -4.91623E-02   6.45960E+01   -9.97673E+00   4.05869E+02
    0.3376       2.96210E+00   1.00000E+00   0.00000E+00   9.00000E+01   -3.32344E-02   6.25630E+01   -6.53213E+00   3.93095E+02
    0.3122       3.20323E+00   1.00000E+00   0.00000E+00   9.40000E+01   -8.11910E-03   6.04246E+01   -1.54124E+00   3.79659E+02
    0.2888       3.46247E+00   1.00000E+00   0.00000E+00   9.80000E+01    2.85092E-02   5.82793E+01    5.21975E+00   3.66180E+02
    0.2678       3.73375E+00   1.00000E+00   0.00000E+00   1.02000E+02    7.58472E-02   5.62509E+01    1.34035E+01   3.53435E+02
    0.2492       4.01290E+00   1.00000E+00   0.00000E+00   1.06000E+02    1.29423E-01   5.43904E+01    2.21148E+01   3.41745E+02
    0.2324       4.30211E+00   1.00000E+00   0.00000E+00   1.10000E+02    1.84699E-01   5.26484E+01    3.05493E+01   3.30800E+02
    0.2170       4.60781E+00   1.00000E+00   0.00000E+00   1.14000E+02    2.39228E-01   5.09430E+01    3.82865E+01   3.20085E+02
    0.2025       4.93795E+00   1.00000E+00   0.00000E+00   1.18000E+02    2.91906E-01   4.92050E+01    4.51235E+01   3.09164E+02
    0.1886       5.30145E+00   1.00000E+00   0.00000E+00   1.22000E+02    3.41814E-01   4.73849E+01    5.08838E+01   2.97728E+02
    0.1752       5.70807E+00   1.00000E+00   0.00000E+00   1.26000E+02    3.87333E-01   4.54523E+01    5.53083E+01   2.85585E+02
    0.1621       6.16714E+00   1.00000E+00   0.00000E+00   1.30000E+02    4.25290E-01   4.34044E+01    5.79921E+01   2.72718E+02
    0.1496       6.68252E+00   1.00000E+00   0.00000E+00   1.34000E+02    4.50265E-01   4.12894E+01    5.84060E+01   2.59429E+02
    0.1381       7.24176E+00   1.00000E+00   0.00000E+00   1.38000E+02    4.55745E-01   3.92382E+01    5.61800E+01   2.46541E+02
    0.1280       7.80981E+00   1.00000E+00   0.00000E+00   1.42000E+02    4.39766E-01   3.74388E+01    5.17242E+01   2.35235E+02
    0.1197       8.35390E+00   1.00000E+00   0.00000E+00   1.46000E+02    4.09908E-01   3.59863E+01    4.63419E+01   2.26109E+02
    0.1127       8.87161E+00   1.00000E+00   0.00000E+00   1.50000E+02    3.76795E-01   3.48148E+01    4.12115E+01   2.18748E+02
```

Table 7 CFA Results For AR=1 and λ=0.7

```
                                       FLUTTER   SUMMARY
                    CONFIGURATION = AEROSG2D     XY-SYMMETRY = ASYMMETRIC      XZ-SYMMETRY = ASYMMETRIC
          POINT =    2    METHOD = PKNL
```

| KFREQ	1./KFREQ	DENSITY	MACH NO.	VELOCITY	DAMPING	FREQUENCY	COMPLEX	EIGENVALUE
0.5256	1.90255E+00	1.00000E+00	0.00000E+00	1.00000E+01	-8.90921E-02	1.08641E+01	-3.04076E+00	6.82610E+01
0.2831	3.53291E+00	1.00000E+00	0.00000E+00	1.40000E+01	1.62226E-01	8.19077E+00	4.17442E+00	5.14641E+01
0.1691	5.91359E+00	1.00000E+00	0.00000E+00	1.80000E+01	8.22289E-01	6.29145E+00	1.62527E+01	3.95303E+01
0.0871	1.14827E+01	1.00000E+00	0.00000E+00	2.20000E+01	1.89347E+00	3.96010E+00	2.35567E+01	2.48820E+01
0.0000	1.00000E+25	1.00000E+00	0.00000E+00	2.60000E+01	4.83222E-01	0.00000E+00	5.65484E+01	0.00000E+00
0.0000	1.00000E+25	1.00000E+00	0.00000E+00	3.00000E+01	6.10659E-01	0.00000E+00	8.24556E+01	0.00000E+00
0.0000	1.00000E+25	1.00000E+00	0.00000E+00	3.40000E+01	6.78408E-01	0.00000E+00	1.03817E+02	0.00000E+00
0.0000	1.00000E+25	1.00000E+00	0.00000E+00	3.80000E+01	7.21071E-01	0.00000E+00	1.23328E+02	0.00000E+00
0.0000	1.00000E+25	1.00000E+00	0.00000E+00	4.20000E+01	7.50219E-01	0.00000E+00	1.41820E+02	0.00000E+00
0.0000	1.00000E+25	1.00000E+00	0.00000E+00	4.60000E+01	7.71199E-01	0.00000E+00	1.59670E+02	0.00000E+00
0.0000	1.00000E+25	1.00000E+00	0.00000E+00	5.00000E+01	7.86878E-01	0.00000E+00	1.77083E+02	0.00000E+00
0.0000	1.00000E+25	1.00000E+00	0.00000E+00	5.40000E+01	7.98940E-01	0.00000E+00	1.94182E+02	0.00000E+00
0.0000	1.00000E+25	1.00000E+00	0.00000E+00	5.80000E+01	8.08438E-01	0.00000E+00	2.11045E+02	0.00000E+00
0.0000	1.00000E+25	1.00000E+00	0.00000E+00	6.20000E+01	8.16062E-01	0.00000E+00	2.27727E+02	0.00000E+00
0.0000	1.00000E+25	1.00000E+00	0.00000E+00	6.60000E+01	8.22281E-01	0.00000E+00	2.44267E+02	0.00000E+00
0.0000	1.00000E+25	1.00000E+00	0.00000E+00	7.00000E+01	8.27427E-01	0.00000E+00	2.60692E+02	0.00000E+00
0.0000	1.00000E+25	1.00000E+00	0.00000E+00	7.40000E+01	8.31735E-01	0.00000E+00	2.77024E+02	0.00000E+00
0.0000	1.00000E+25	1.00000E+00	0.00000E+00	7.80000E+01	8.35382E-01	0.00000E+00	2.93278E+02	0.00000E+00
0.0000	1.00000E+25	1.00000E+00	0.00000E+00	8.20000E+01	8.38499E-01	0.00000E+00	3.09469E+02	0.00000E+00
0.0000	1.00000E+25	1.00000E+00	0.00000E+00	8.60000E+01	8.41185E-01	0.00000E+00	3.25604E+02	0.00000E+00
0.0000	1.00000E+25	1.00000E+00	0.00000E+00	9.00000E+01	8.43517E-01	0.00000E+00	3.41693E+02	0.00000E+00
0.0000	1.00000E+25	1.00000E+00	0.00000E+00	9.40000E+01	8.45557E-01	0.00000E+00	3.57743E+02	0.00000E+00
0.0000	1.00000E+25	1.00000E+00	0.00000E+00	9.80000E+01	8.47353E-01	0.00000E+00	3.73758E+02	0.00000E+00
0.0000	1.00000E+25	1.00000E+00	0.00000E+00	1.02000E+02	8.48942E-01	0.00000E+00	3.89743E+02	0.00000E+00
0.0000	1.00000E+25	1.00000E+00	0.00000E+00	1.06000E+02	8.50356E-01	0.00000E+00	4.05702E+02	0.00000E+00
0.0000	1.00000E+25	1.00000E+00	0.00000E+00	1.10000E+02	8.51622E-01	0.00000E+00	4.21638E+02	0.00000E+00
0.0000	1.00000E+25	1.00000E+00	0.00000E+00	1.14000E+02	8.52758E-01	0.00000E+00	4.37553E+02	0.00000E+00
0.0000	1.00000E+25	1.00000E+00	0.00000E+00	1.18000E+02	8.53784E-01	0.00000E+00	4.53451E+02	0.00000E+00
0.0000	1.00000E+25	1.00000E+00	0.00000E+00	1.22000E+02	8.54713E-01	0.00000E+00	4.69333E+02	0.00000E+00
0.0000	1.00000E+25	1.00000E+00	0.00000E+00	1.26000E+02	8.55558E-01	0.00000E+00	4.85200E+02	0.00000E+00
0.0000	1.00000E+25	1.00000E+00	0.00000E+00	1.30000E+02	8.56329E-01	0.00000E+00	5.01054E+02	0.00000E+00
0.0000	1.00000E+25	1.00000E+00	0.00000E+00	1.34000E+02	8.57035E-01	0.00000E+00	5.16896E+02	0.00000E+00
0.0000	1.00000E+25	1.00000E+00	0.00000E+00	1.38000E+02	8.57682E-01	0.00000E+00	5.32728E+02	0.00000E+00
0.0000	1.00000E+25	1.00000E+00	0.00000E+00	1.42000E+02	8.58279E-01	0.00000E+00	5.48551E+02	0.00000E+00
0.0000	1.00000E+25	1.00000E+00	0.00000E+00	1.46000E+02	8.58829E-01	0.00000E+00	5.64365E+02	0.00000E+00
0.0000	1.00000E+25	1.00000E+00	0.00000E+00	1.50000E+02	8.59339E-01	0.00000E+00	5.80171E+02	0.00000E+00
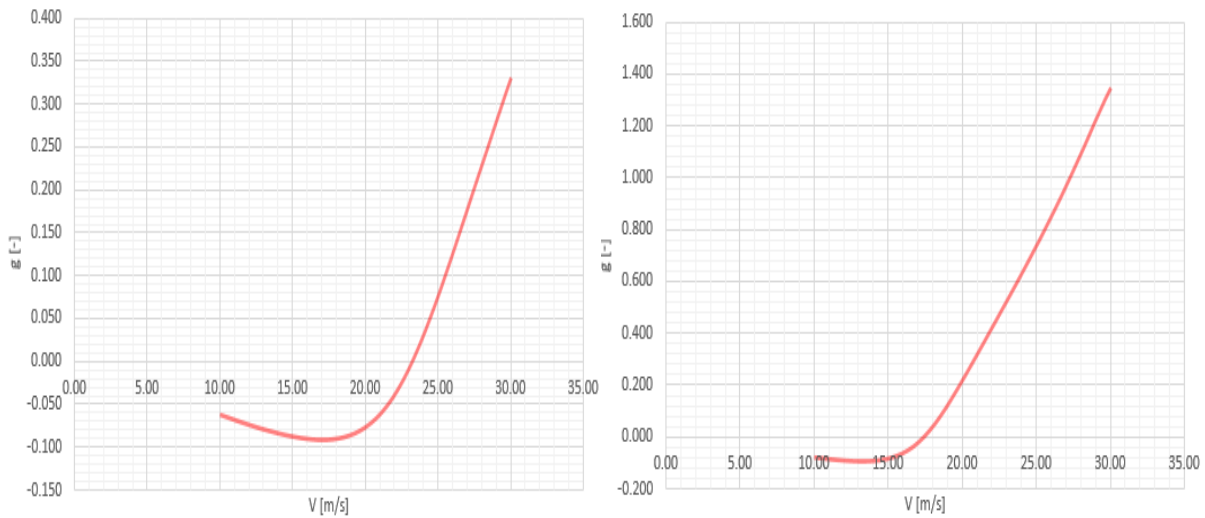
Figure 14. Effect of material on flutter speeds, EGlass/Epoxy and Carbon Epoxy

4. CONCLUSION

The effects of taper and aspect ratio of thin plates and shells are investigated from the static and dynamic stability point of view. These structures are the building block of any modern flight-worthy airframe, and stability is of great concern and has to be performed even in the early stages of the design.

If modern composite materials are used, current and existing theories for static torsional divergence pheno–mena and for dynamic flutter have to be modified in order to take the material anisotropy into account since it was found that material characteristics highly influence the flutter and divergence speeds. Ackerman QI theory for composite plates is used and presented in this paper. It can be concluded that this approach renders relatively good results for torsional divergence speeds and flutter speeds and is less computationally involved when compared to the CFA approach. Further, based on this analysis, it can be concluded that the methodology for stability analysis, for both static and dynamic, presented can be used in the preliminary stages of the design and used with relatively moderate computational expenses. Variations in aspect ratios of the tapered plate highly influence the overall stability, whereas the variations of the taper ratio influence the

stability as well to a lesser extent. If the structures are designed from modern composite materials, a greater number of material characteristics have to be considered, which requires more complex analytic and numeric analyses; however, this potentially leads to more efficient and more optimal airframe designs.

Optimization of the structures analyzed in this paper, due to a great number of parameters, represents a chal–lenging task and is a recommendation for future work.

REFERENCES

[1] Zhang, L., Wang, X., Pei, J., & Zhou, Y.: Review of automated fiber placement and its prospects for advanced composites. Journal of Materials Science, 1–35, (2020).

[2] Rodney H. Ricketts.: Structural Testing for Static Failure, Flutter, and Other Scary Things, Langley Research Center, 1983

[3] Y C, Fung.: An Introduction to the Theory of Aeroelasticity, Dover Books on Aeronautical Engineering,1955

[4] John K. Ramsey.: NASA Aeroelasticity Handbook Volume 2: Design Guides, NASA/TP—2006-212490/VOL2/PART2, 2006

[5] Rama B. Bhat.: Principles of Aeroelasticity, CRC Press Taylor & Francis Group, 2016

[6] R L. Bisplinghoff, Holt Ashley.: Principles of Aeroelasticity, Dover Books on Engineering 2nd edition, 2013

[7] Dinulović, M., Rašuo, B., Slavković, A., Zajić, G.: Flutter analysis of tapered composite fins: Analysis and experiment, FME Transactions, vol. 50, No. 3, pp. 576-585, 2022

[8] Neill, D.J., and Sikes, G.: The MSC Flight Loads System, MSC Aerospace User's Conference, November 1997

[9] Rodden, William P., and Johnson, Erwin H.: MSC/NASTRAN Aeroelastic Analysis User's Guide, V68, The MacNeal-SchwendlerCorporation, 1994

[10] Johnson, E.H. and Rodden, W.P.: "Ongoing Development of the MSC/NASTRAN Aeroelastic Capability," presented at the 17thMSC European User's Conference, Paris, France, Sept. 199

[11] Raymond L. Bisplinghoff, Holt Ashley, Robert L. Halfman.: Aeroelasticity (Dover Books on Aeronautical Engineering), 1983

[12] Karthik Menon and Rajat Mittal.: Computational Modeling and Analysis of Aeroelastic Wing Flutter, AIAA AVIATION Forum, June 25-29, 2018, Atlanta, Georgia

[13] Fadlalla, AAM., Sahin, AZ., Ouakad, HM., Bahaidarah, H.: Aeroelastic Analysis of Straight-bladed Vertical Axis Wind Turbine Blade, FME Transactions, Vol. 50, No. 3, pp. 512-525, 2022,

[14] Ji Wang.: The extended Rayleigh-Ritz method for analysis of nonlinear vibrations, Mechanics Of Advanced Materials And Structures, 2021

[15] Ian H. Sloan.: Four Variants of dying Galerkin Method for Integral Equations of the Second Kind, IMA Journal of Numerical Analysis (1984)

[16] Daniel, I.: Engineering Mechanics of Composite Materials, Oxford University Press, 1994

[17] Dinulovic, M., Rašuo, B., Krstic, B.: The Analysis of Laminate Lay-Up Effect on the Flutter Speed of Composite Stabilizers, The International Council of the Aeronautical Sciences - The 30th ICAS Congress 25-30. September 2016, Daejeon, Korea, https://www.icas.org/ICAS_ARCHIVE/ICAS2016/data/papers/2016_0271_paper.pdf

[18] Massard, T.: Computer sizing of composite laminates for strength, Journal of Reinforced Plastics and Composites, 3(4), (1984)

[19] P Bortolotti1, G Adolphs and C L Bottasso.: Methodology to guide the selection of composite materials in a wind turbine rotor blade design process, Journal of Physics: Conference Series 753 (2016)

[20] Akkerman, R.: *On the properties of quasi-isotropic laminates*, Composites: Part B, Vol. 33 (2002) pp. 133-40.

[21] Gabriela Stroe, Irina-Carmen Andrei, Tiberiu Adrian Salaoru.: Dynamic Performances of the Automatic Flight Control System, 5th International Workshop on Numerical Modelling in Aerospace Sciences, NMAS 2017,17-18 May 2017, Bucharest, Romania

[22] Barrowman, James S.: The Practical Calculation of the Aerodynamic Characteristics of Slender Finned Vehicles, NASA/TM-2001-209983

АНАЛИЗА УТИЦАЈА ВИТКОСТИ И СУЖЕЊА НА АЕРОЕЛАТИЧНУ СТАБИЛОНСТ КОМПОЗИТНИХ ЉУСКИ

М. Динуловић, Б. Рашуо, Н. Славковић, Ђ. Карић

У овом раду анализирана је статичка и динамичка стабилност, за различите аеродинамичке конфигурације композитних плоча. На основу посојећих модела за флатер и торсиону дивергенцију, модификованих како би била узета у обзир анизотропија материјала, коефицијенти стабилности су израчунати за различите виткости и сужења узгонских и управљачких површина. Може бити закључено да је приказана методологија веома ефикасна нарочито у прелиминарним фазама пројеката када је потребно изанлизирати велики број потенцијалних конфигурација са аеродинамичког аспекта за различите случајеве лета.